Peak ground velocity ShakeMaps derived from geodetic slip models

Junkee Rhie,[1] Douglas S. Dreger,[2] Mark Murray[3] and Nicolas Houlié[2,*]

[1]*School of Earth and Environmental Science, Seoul National University, Seoul 151-742, Korea. E-mail: rhie@snu.ac.kr*
[2]*Berkeley Seismological Laboratory, University of California, Berkeley, CA 94720, CA, USA*
[3]*Department of Earth and Environmental Science, New Mexico Institute of Mining and Technology, Socorro, NM 87801, USA*

SUMMARY

We develop a methodology to derive fast and reliable peak ground velocity (PGV) ShakeMaps from kinematic finite-source models of earthquake rupture inferred from geodetic static displacements. The temporal variations in slip on the fault are based on the simple assumption that larger slip takes longer time to accumulate. Assuming constant rupture and slip velocities, slip is distributed in time to produce a variable rise-time model. Sensitivity tests on finite-source models of the 1994 M_w 6.7 Northridge, California earthquake show that distribution of peak ground velocities derived using 3.0 km s^{-1} rupture velocity and 76.8 cm s^{-1} slip velocity matches, to a large extent, observed PGV, suggesting that rapid assessment of strong ground motions derived from geodetic data can aid emergency response, particularly in areas with sparse seismic station coverage.

Key words: Satellite geodesy; Earthquake ground motions; Site effects.

1 INTRODUCTION

Accurate estimation of near-fault strong ground motion from our basic understanding of faulting mechanisms and seismic wave propagation is an important goal in earthquake engineering. Peak ground motion distributions provide information that may be used to assess earthquake impacts. In areas where there are no near-fault recordings of strong ground motions, such rapid source model based estimations can be crucial in producing a strong ground motion ShakeMap (Wald *et al.* 1999) or augmenting ShakeMap in sparse recording situations (e.g. Dreger & Kaverina 2000; Dreger *et al.* 2005). Determination of strong ground motions using a representation theorem that includes a space–time convolution of slip and Green's functions (Burridge & Knopoff 1964) has become commonplace for characterizing kinematic source parameters following large earthquakes (e.g. Hartzell & Heaton 1983; Wald & Heaton 1994; Kaverina *et al.* 2002), and has been applied rapidly after earthquake occurrence (e.g. Dreger & Kaverina 2000; Hardebeck *et al.* 2004), and the finite extent of rupture from such models has been used to improve strong ground motion estimates in areas lacking direct observation of the strong motions (Dreger *et al.* 2005).

The form of the representation theorem implies that strong ground motions cannot be reliably predicted without knowing both the spatio-temporal slip history and the Green's function describing seismic wave propagation from source to receiver. With rapidly determined static GPS deformation information joint inversions of seismic waveforms and static deformation can provide better con-

strained kinematic models (e.g. Kaverina *et al.* 2002; Rolandone *et al.* 2006).

GPS data can be used to independently determine the faulting orientation and slip distribution, and inversions of GPS data can be more rapidly performed. Such GPS slip models give no information on the timing of the slip, which is required in order to simulate near-fault strong ground motions. The GPS slip models can be used directly by providing information on the finite extent of the fault rupture, or by interpreting the relative position of the seismically determined hypocentre with respect to the slip distribution to infer the degree of directivity. GPS slip models cannot be used to directly simulate near-fault strong ground motions, and in order to do so a method for describing the rupture kinematics is needed. In this paper, we investigate a method of generating a kinematic model of the fault process based on the slip distribution from the inversion of GPS static displacements.

The main goal of this study is to develop a deterministic method to simulate temporal variations of slip from geodetic static displacements, and apply this method to derive rapid and reliable near-fault ShakeMaps for earthquakes. Geodetic observations offer several advantages. Geodetic inversions can independently determine the orientation and fault finiteness quickly, whereas seismic inversions must first determine a moment tensor, and then test both possible nodal planes. Because geodetic slip-model inversions take less computer time than seismic inversions, this method can more quickly predict a level of shaking when real-time GPS observations are available.

In case of the San Francisco Bay Area (SFBA), the distribution of current real time GPS stations is dense enough to invert displacements due to a local earthquake with magnitude larger than around 6.5 for slip distribution on a fault plane. The processing

GJI Seismology

time to obtain final GPS value from real time GPS measurement is about 2–20 min while the time, mainly depending on the performance of the processor, to invert those to final average slip model, it is less than 2 min (e.g. Clarke *et al.* 1997; Wright *et al.* 1999). For emergency response, even a small improvement in time can be significant. Available geodetic data can be included with available seismic waveform data in joint inversions for slip, which provides greater constraint on the kinematic source process (e.g. Kaverina *et al.* 2002). Geodetic data sets also provide redundancy should seismic data sets be sparse or inaccessible in real-time, or difficulties arise in the multistage processing of the seismic data as carried out using the method of Dreger & Kaverina (2000) and Dreger *et al.* (2005). The combination of the two data types and their independent or joint inversion is a crucial next step in developing robust automated procedures to characterize finite-fault rupture parameters for use in rapid strong ground motion reporting.

2 SPATIO-TEMPORAL SLIP MODEL

Our method for deriving a spatio-temporal slip model from static dislocations is based on the intuitive assumption that larger slip takes longer time to accumulate. This assumption follows from a self-similar scaling relation between rise time and slip. A dislocation rise time increases in proportion to slip and it indicates that slip velocity is constant. Even though recent studies have showed that many factors control slip velocity, such as stress drop and strength (e.g. Oglesby & Day 2002), we assume a constant slip velocity over the fault on average for its simplicity in the rapid estimation of the level of the shaking. This simple self-similar scaling model seems to describe the average properties of rupture well. Somerville *et al.* (1999) developed empirical scaling relations between dislocation rise time, average slip and moment for crustal earthquakes. We obtain a constant slip velocity of 76.8 (cm s^{-1}) from their self-similar relations. This value may not be exactly true for the specific earthquakes, however it gives an idea of the order of magnitude of slip velocity for crustal earthquakes.

The kinematic rupture model we employ describes a spatially variable slip model that is defined by a grid of point sources on a fault plane with rupture duration given by multiple time windows, following the method of Hartzell & Heaton (1983). We define the average rise time by using the relationship $T_r = 4.37 \times 10^{-7} M_o^{1/3}$ (here the unit of seismic moment is N m) (Somerville *et al.* 1999). Scalar seismic moment M_o is assumed to be known *a priori*, either from seismic or geodetic estimates. We define the minimum rise time in the model to be $T_r/2$, which specifies the duration of the unit source time function or time window. The regions with the smallest slip take the minimum rise time to finish slipping, while the regions with larger slip require multiple time windows, which are staggered by half of the minimum rise time (Fig. 1). The number of time windows for each point source is based on the ratio of the spatially variable slip to the constant slip velocity. For a given level of slip, a larger assumed slip velocity implies that more slip occurs in each of the time windows resulting in a shorter overall duration.

In the model a circular rupture front initiates at the hypocentre and propagates with constant assumed rupture velocity. Slip is triggered when the rupture front reaches each point source and has a duration determined by the number of time windows appropriate for the level of slip at that point. We assume the hypocentre is known *a priori* from seismic estimates. For events in California, the hypocentre is typically determined within 30–120 s after the occurrence of the earthquake (Gee *et al.* 2003), substantially before near-realtime GPS data would be available for processing. Although it is impossible to know *a priori* how the rupture velocity will vary or what it will be on average, a commonly reported value is approximately 80–90 per cent of the shear wave velocity.

## 3 THE NORTHRIDGE EARTHQUAKE EXAMPLE

We demonstrate the method by simulating peak ground velocity (PGV) ground motion maps from three slip models for the 1994 January 17 M_w 6.7 Northridge earthquake (see Table 1). Model REF (reference), determined by inverting near-source strong ground motions, P and SH teleseismic body waves, and GPS and spirit levelling geodetic data (Wald *et al.* 1996), provides reference PGV for comparison with PGV obtained from the source models inferred from
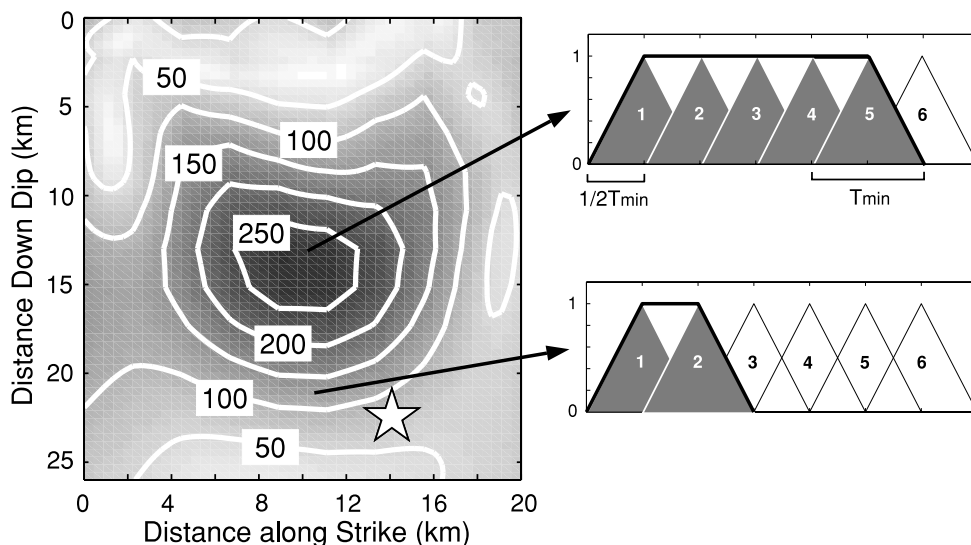
Figure 1. A schematic diagram showing how to determine the number of time windows for a variable-slip model. Left-hand column shows the variable slip model on its rupture plane (Hudnut *et al.* 1996). White star indicates hypocentre of Northridge event. Two small panels on the right-hand side indicate necessary time windows (solid grey triangles) and final rise time curve (thick black) associated with slip patches indicated on slip distribution model.

Table 1. Three finite-fault model parameters.

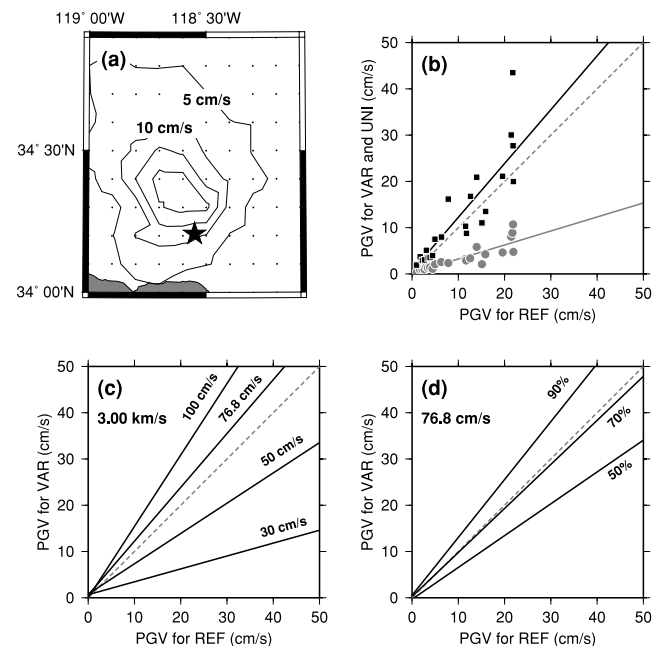| Model	Strike (°)	Dip (°)	Average rake (°)	Top centre [Lat/Lon/Depth (km)]	Length/width (km)	Max./Ave. slip (m)
REF	122	40	101	34.345/−118.515/5.103	18/24	3.12/1.3
VAR	109.6	41	91.3	34.364/−118.529/1.000	20/26	2.81/1.0
UNI	109.13	39.22	89.17	34.318/−118.558/7.770	7.11/12.19	4.5213/4.5213
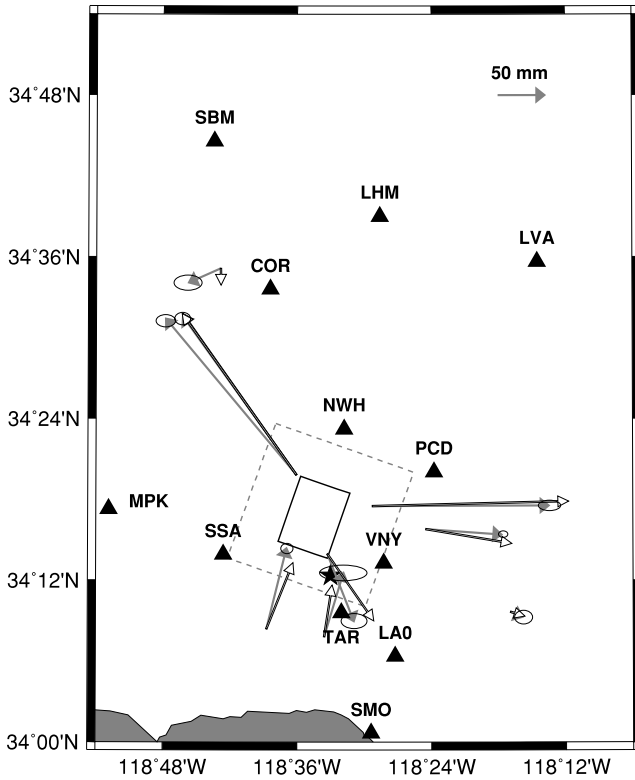
Figure 2. A comparison of observed (grey), with 95 per cent confidence regions, and modelled (white) GPS displacement vectors in the vicinity of the epicentre (black star). Rectangles and surface projection of the finite-fault geometries for the uniform-slip inversion based on 10 GPS displacement (thick solid, Hudnut & Murray 1994, personal communication) and the variable-slip inversion from seismic and geodetic observation (dotted grey) (Hudnut *et al.* 1996). 12 selected stations are indicated with black triangles.

slip velocity is 76.8 cm s^{-1}. The two geodetic models UNI and VAR have seismic moments of 1.3715×10^{19} and 1.8985×10^{19} N m corresponding to minimum rise time functions of 0.523 and 0.583 s, respectively. Given the maximum slip in each of these models (452.13 and 281.01 cm), 22 and 12 time windows are used in each model to distribute the slip in time. The final rise time as parametrized can differ from the estimated rupture time (dividing slip by slip velocity) because of the fixed duration of the unit time window. However this difference has no significant impact on the simulated ground motions. For model REF, we used the parameters for rise time and the slip time window distribution reported by Wald *et al.* (1996). To reduce artefacts from coarse discretization, the slip models were interpolated so that the rupture time across a subfault is much less than the minimum rise time. The final spatio-temporal slip models have the same scalar seismic moments and slip distribution derived from the geodetic inversions, but have that slip distributed in time.

To assess the methodology, we compare predicted PGV for model REF and two other GPS-only models (VAR and UNI) at an artificial grid in the region (34–35°N and 118–119°E) with the interspacing of 0.1° in both longitude and latitude. The waveforms for each source model were simulated using Green's function for Wald's rock

geodetic data only. Model UNI was obtained by a non-linear inversion method for fault orientation, dimension and uniform slip using 10 GPS displacement vectors (Fig. 2) measured in the first week after the main shock (Hudnut & Murray 1994, personal communication 1994). Model VAR was obtained from a non-linear inversion for fault plane geometry followed by a linear inversion for variable slip on the estimated fault plane (Hudnut *et al.* 1996).

We assume that rupture initiated near the hypocentre (34.206°N, 118.550°W, 17.5 km depth) obtained independently from the short-period seismic network (Hauksson *et al.* 1995). Because the fault planes used in the two geodetic slip models do not include the hypocentre, we initiated rupture at the point of intersection of a vertical line from the seismic hypocentre on the geodetic-derived fault planes. If the fault plane is too small to include the point of intersection, we extended the fault plane to include the point but no slip is assumed on the extended part of the fault. Future applications can solve for finite-source parameters with the constraint that the fault plane must include the hypocentre. We assume that the constant

Figure 3. (a) A predicted PGV ShakeMap for model REF. The black dots are the grid locations where strong motions are derived for ShakeMap. The black star indicates main shock epicentre. (b) A comparison of PGV for two geodetic models (VAR and UNI) and model REF. For the reference, the perfect agreement line is indicated with the dotted grey line. (c) The best fitting lines assuming different slip velocities for constant rupture velocity of 3.0 km s^{-1}. (d) The best fitting lines assuming different rupture velocities for constant slip velocity of 76.8 cm s^{-1}.
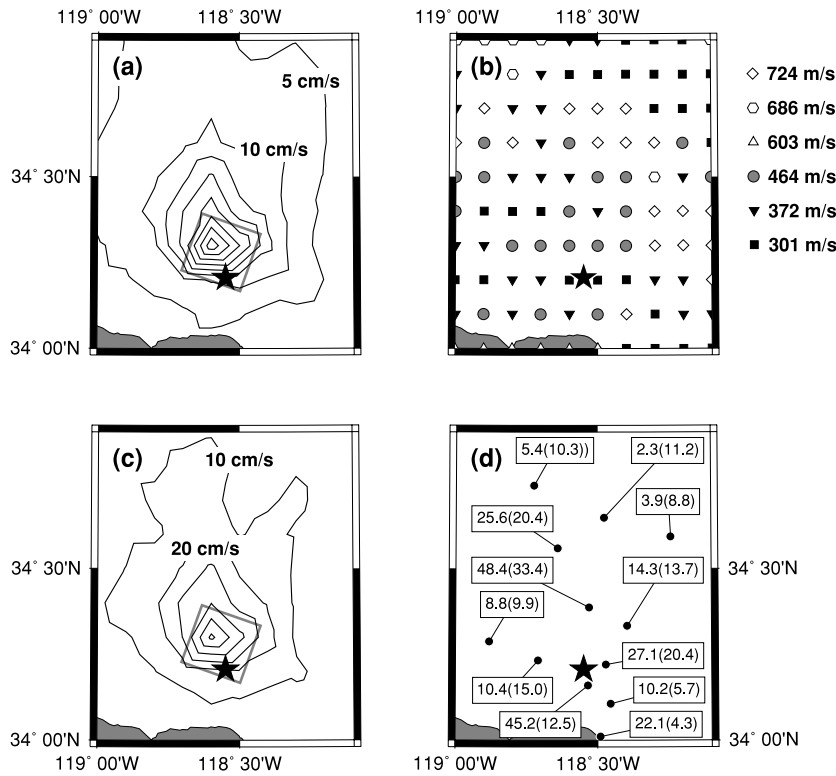
Figure 4. (a) A predicted PGV ShakeMap for model VAR within a slip velocity of 76.8 cm s^{-1} and rupture velocity of 3.00 km s^{-1} assumptions. The black star indicates main shock epicentre. Rectangles are surface projection of model VAR. (b) An average upper 30 m shear wave velocities at grid points within given region. (c) Same as (a) for after correcting site effects. (d) A comparison of predicted PGV and observed PGV at 12 stations. Figures in box and parenthesis refer to observed and predicted PGV in cm s^{-1}.

Table 2. Observed and predicted PGV at 12 selected stations.

Station	Latitude (°)	Longitude (°)	Observed PGV (cm s^{-1})	Predicted PGV^a (cm s^{-1})	Predicted PGV^b (cm s^{-1})
COR	34.560	−118.640	25.6	20.4	7.3
LA0	34.106	−118.454	10.2	5.7	1.7
LHM	34.650	−118.477	2.3	11.2	3.0
LVA	34.594	−118.242	3.9	8.8	2.8
MPK	34.228	−118.881	8.8	9.9	1.9
NWH	34.387	−118.530	48.4	33.4	9.9
PCD	34.334	−118.396	14.3	13.7	3.1
SBM	34.743	−118.724	5.4	10.3	2.8
SSA	34.232	−118.710	10.4	15.0	4.4
SMO	34.011	−118.490	22.1	4.3	2.5
TAR	34.160	−118.543	45.2	12.5	3.4
VNY	34.221	−118.471	27.1	20.4	4.2

Note: PGV is computed from the waveform low-pass filtered with the corner frequency of 1 Hz.
^{a}Model VAR.
^{b}Model UNI.

model (Wald *et al.* 1996) that has a minimum shear wave velocity of 1 km s^{-1}. A predicted waveform is low-pass filtered with the corner frequency of 1 Hz. PGV is computed by taking the geometric mean of two horizontal peak ground velocities at each grid point. We chose to use the geometric mean of the horizontal components, because attenuation models of ground motions commonly give results in terms of the geometric mean. To quantify our assessment, we calculated the best fitting lines of simulated PGV for model VAR and UNI as a function of predicted PGV for model REF. The slopes of the best fitting lines are 0.30 and 1.16 for models UNI and VAR. The PGV values derived from model UNI are significantly less than

the predicted PGV from model REF, which is inverted from seismic waveforms, possibly because the model is too smooth and spread out in time. The simulated PGV for model VAR tends to be slightly larger than model REF, but the difference is not significant (Figs 3a and b). This assessment indicates that even though the real slip velocity is not constant over the fault plane, the level of shaking around the fault plane can be, to a large extent, estimated by only assuming constant slip velocity derived from empirical relations.

We tested the sensitivity of the simulated PGV for model VAR to slip velocity by assuming 30, 50, 76.8 and 100 cm s^{-1}, and a constant rupture velocity of 3.0 km s^{-1} (86 per cent of assumed 3.5 km s^{-1}
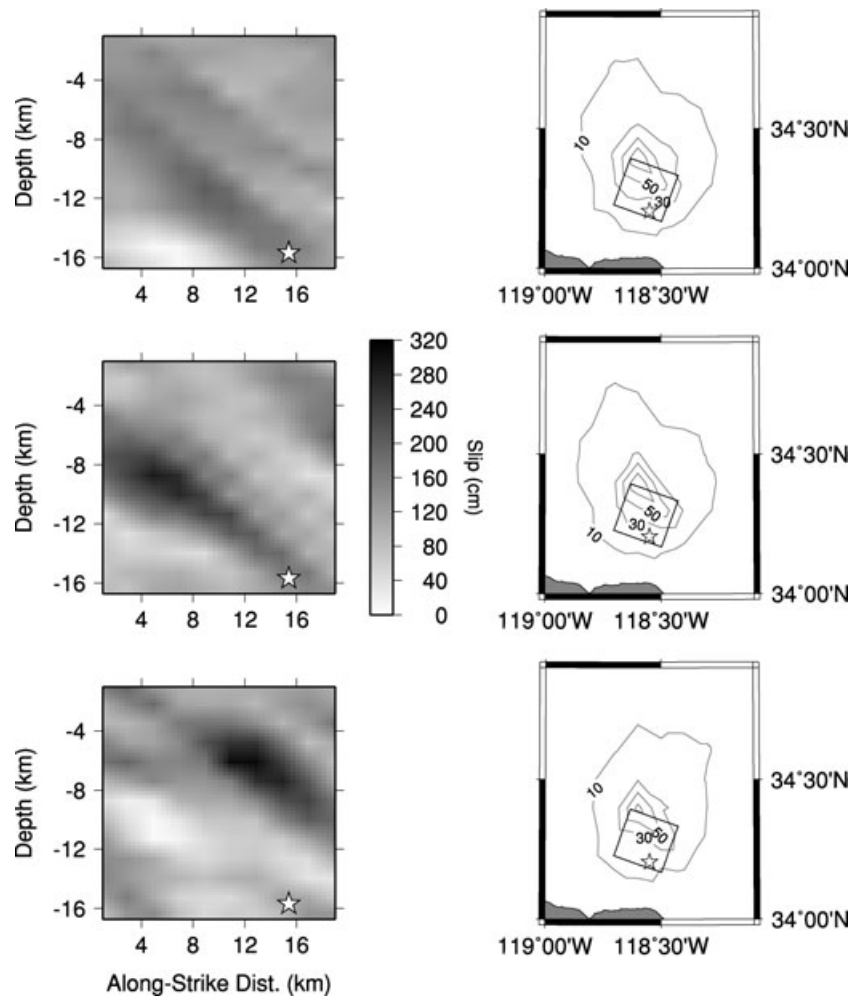
Figure 5. A sensitivity test for random slip models. Left-hand panels: three random slip models computed using the method of Mai & Beroza (2002). Right-hand panels: associating ShakeMaps for the slip model on the left-hand side. No amplification factor is applied. ShakeMaps are more or less consistent with different slip models.

shear wave velocity) (Fig. 3c). For a given rupture velocity, the level of PGV increases with slip velocity and slip velocity between 50 and 76.8 cm s^{-1} agree well with the predicted level of PGV for model REF. We also tested the sensitivity of PGV to the assumed rupture velocity for a constant slip velocity of 76.8 cm s^{-1} using 1.80, 2.45, and 3.15 km s^{-1}, which are 50, 70 and 90 per cent of the shear wave velocity (Fig. 3d). The level of PGV increases with rupture velocity and rupture velocity between 70 and 90 per cent of shear wave velocity are appropriate to predict the level of PGV for model REF.

We find that simulated PGV for the time varying slip model is comparable to PGV for the model directly derived from seismic data. We compared the predicted PGV for our estimated slip model to the real observed PGV (Fig. 4) and find that the simulated PGV agrees reasonably well with the observations. As we mentioned before, it is important to have good Green's functions to predict waveforms. However, we are just interested in the level of PGV rather than waveform itself. Therefore, we just use 1-D Green's functions for Wald's rock model (Wald *et al.* 1996) and then correct PGV for site effects.

To account for site effects, we applied site amplification factors to the waveforms based on the upper 30 m shear wave velocity (Wills *et al.* 2000) as is done in the NEHRP site classification

system (Borcherdt 1994). Amplification factors are calculated by considering differences in impedances at surface for the rock model and given site for a normal incidence seismic wave.

$$A = \frac{2\rho_r \beta_r}{\rho_s \beta_s + \rho_r \beta_r},$$

where A is amplification factor. ρ_r and ρ_s are density at the surface and β_r and β_s are shear wave velocity at the surface for Wald's rock model (1.8 g cm^{-3} and 1.00 km s^{-1}) and given site, respectively. Here density at given site is determined following empirical relations (Brocher 2005, see his eqs 1 and 9). Simulated PGV ShakeMaps for models VAR and UNI within a constant slip velocity of 76.8 cm s^{-1} and rupture velocity of 3.00 km s^{-1} assumptions, derived from the geometric mean of the two horizontal-component synthetic velocities and corrected for amplification factors, were compared to observed PGV at 12 stations (see Table 2 and Fig. 2) around the epicentre (Fig. 4). The comparison shows that while predicted PGV values from model UNI significantly under predict observed PGV values at most stations, predicted PGV values from model VAR agree well with observed PGV values except at a couple of the stations located to the south of the epicentre, where the observed PGV is larger than predicted by a factor of at least 3 (Fig. 4d). This discrepancy is likely due to very complex 3-D wave
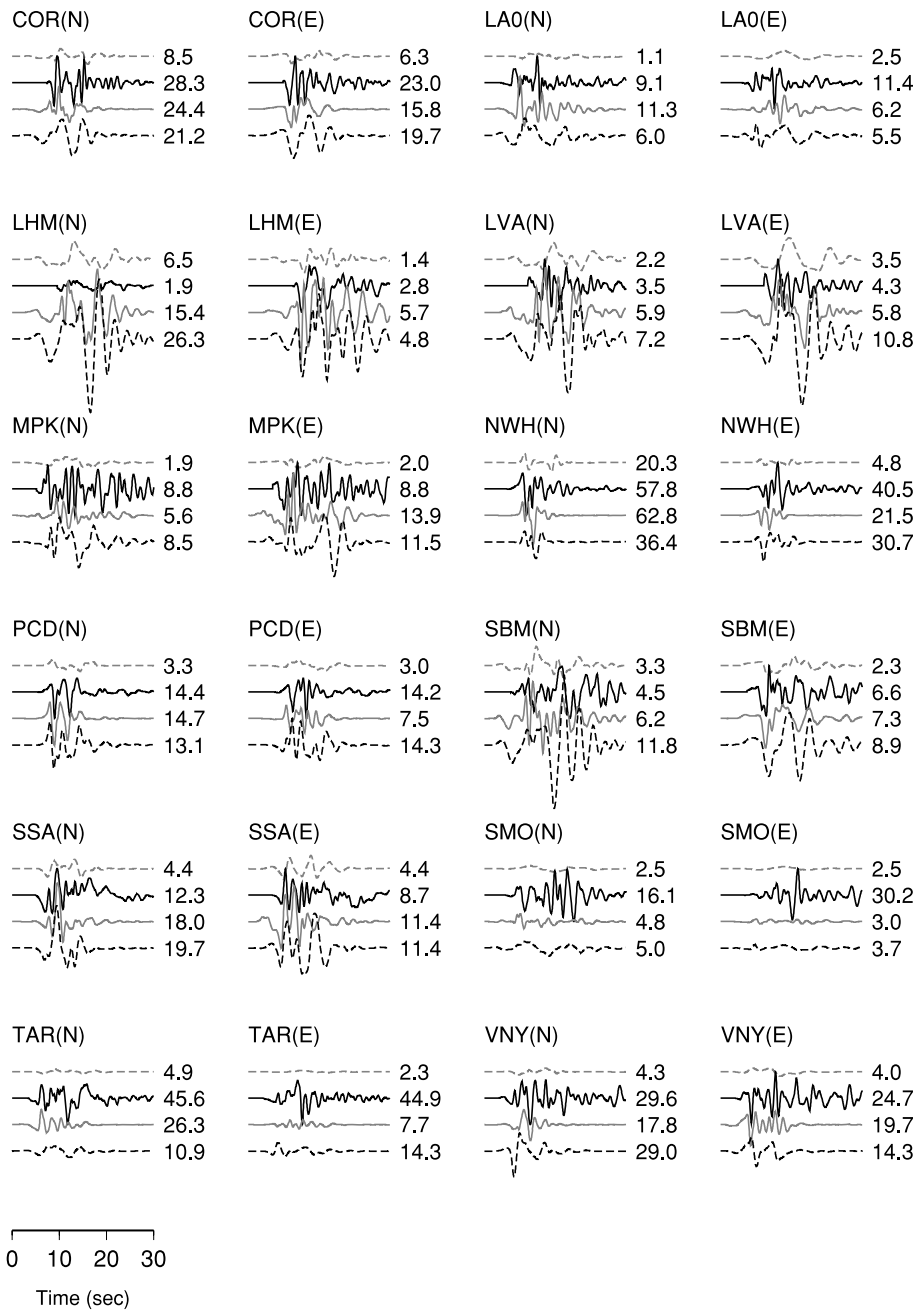
Figure 6. A comparison of two horizontal velocity waveforms at 12 stations (see Fig. 2). Each panel has four waveforms; from the top to bottom, synthetic for model UNI (dotted grey), observation (black), synthetic for models REF (grey) and VAR (dotted black). All waveforms are low pass filtered with the corner frequency of 1 Hz and normalized to the maximum amplitude of observed record. Numbers on the right-hand side of each waveform indicate maximum velocity of records in cm s^{-1}.

propagation related with Los Angeles basin, which is not properly considered in this study.

4 DISCUSSION AND CONCLUSION

We have developed a methodology to derive PGV ground motion maps from geodetic finite-source models. Since our objective is to develop a method that is practical in a rapid (on the order of 30 min) post-earthquake time frame, we made several simplifying assumptions such as constant slip and rupture velocity. As more information becomes available following an earthquake it may be possible to in-

vert for models to resolve these parameters, but such analysis is not applicable in an automated fashion. Nevertheless, to first order, assuming rupture and slip velocities are constant performs well in describing the overall directivity effect and in simulating PGV for ShakeMap (Wald *et al.* 1999) applications (e.g. Dreger & Kaverina 2000; Dreger *et al.* 2005).

PGV for model UNI, which concentrates slip into a smaller source, tends to underpredict PGV due to both the smooth rupture and long rise time, however such a model is still useful to define source finiteness and directivity, which can be used to update ShakeMaps by correcting distance measures for finiteness

(e.g. Dreger *et al.* 2005) or possibly attenuation relations for directivity (e.g. Somerville *et al.* 1997). Simulated PGV ShakeMaps for model VAR are in good agreement with the general distribution of observed PGV.

The level of simulated PGV is sensitive to the uncertainty in the scalar seismic moment used to determine the minimum rise time function and geodetic slip model. Since the minimum rise time function is proportional to the one-third power of scalar seismic moment, uncertainty in scalar seismic moment does not strongly affect the level of PGV. For example, if the moment was off by a factor of two the minimum rise time would change only by 26 per cent. We tested this effect using random but physically plausible slip models computed using the method of Mai & Beroza (2002), and the MatLab software provided by Martin Mai. For these models we find that the overall levels of PGV are more or less consistent with one another and the results for the Northridge earthquake (Fig. 5). This indicates that uncertainty in the geodetic slip model doesn't severely change the level of predicted PGV if the position of the hypocentre with respect to the slip is nearly the same, or in other words the method we have developed accounts mostly for directivity effects. Since the hypocentre is routinely obtained very quickly before real time GPS processing would be finished the likely scenario for an application would be one in which the slip distribution with respect to hypocentre position will be known. This will provide a first-order of the rupture directivity and the PGV distribution around the source.

To access the limitation of the method, we compared the observed and modelled velocity waveforms at 12 stations and also compared spectral accelerations (Sa) with 5 per cent damping at three periods (0.3, 1 and 3 s) (Figs 6 and 7). Several observed records at southern stations (e.g. SMO and TAR) have large amplitude, late arriving, long-period components that are not explained by our synthetics. These are likely due to surface waves produced by 3-D basins in the Los Angeles area that are not modelled by 1-D plane-layered structure we assumed. Although several waveforms for model VAR are different from observed waveforms, most of the peak velocities for model VAR are comparable to the observed peak velocities. A comparison of spectral acceleration shows that model VAR performs well for Sa at 3 s but under predicts Sa at 1 and 0.3 s periods (Fig. 7). These results indicate that such simulated motions, if obtained rapidly, would be useful in evaluating the strong shaking hazard in terms of PGV or Sa at periods greater than 1 s in the aftermath of a large earthquake.

Future work will test this methodology for other large, well-studied events, such as 2003 San Simeon, 1992 Landers and 2004 Parkfield, to optimize the rules for time variation of slip. The 2004 Parkfield is especially important among these events to test our methodology because the spatial coverage of continuous GPS around the epicentre is good enough to determine the near real-time GPS-only slip distribution model. Combining the optimized rules and near real-time measurement and inversion of GPS displacement vectors can likely reduce the estimation time of the extent of near-fault strong ground shaking used in emergency response activities.
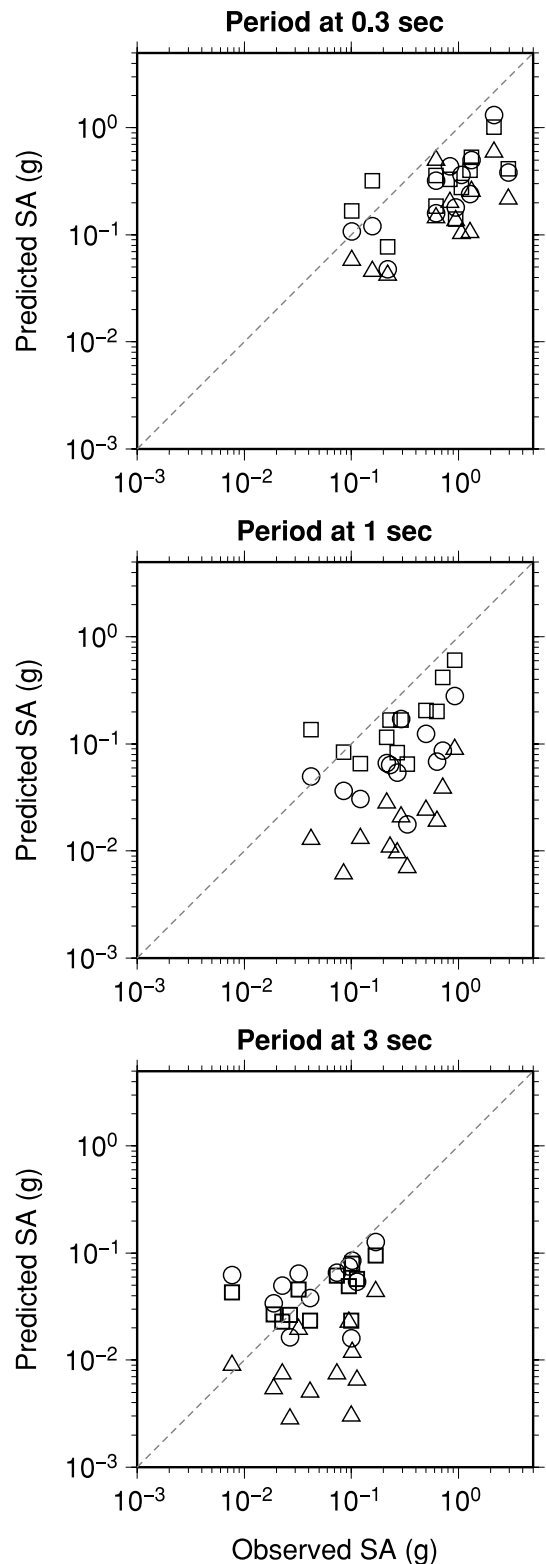
Figure 7. A comparison of the geometric mean of the spectral accelerations (Sa) of the two horizontal components for three models [REF (squares), VAR (circles) and UNI (triangles)] and observation at three periods with 5 per cent damping. Models REF and VAR perform well for Sa at 3 s, and model REF performs well at 1 s. The models under predict Sa at 0.3 s period and shorter.

REFERENCES

Borcherdt, R.D., 1994. Estimates of site-dependent response spectra for design (methodology and justifications), *Earthquake Spectra,* **10,** 617–653.

Brocher, T.M., 2005. Empirical relations between elastic wavespeeds and density in the earth's crust, *Bull. seism. Soc. Am.,* **95**(6), 2081–2092.

Burridge, R. & Knopoff, L., 1964. Body force equivalents for seismic dislocations, *Bull. seism. Soc. Am.,* **54,** 1875–1888.

Dreger, D. & Kaverina, A., 2000. Seismic remote sensing for the earthquake source process and near-source strong shaking: a case study of the October 16, 1999 Hector Mine earthquake, *Geophys. Res. Lett.,* **27**(13), 1941–1944.

Dreger, D.S., Gee, L., Lombard, P., Murray, M.H. & Romanowicz, B., 2005. Rapid finite-source analysis and near-fault strong ground motions: application to the 2003 M_w 6.5 San Simeon and 2004 M_w 6.0 Parkfield earthquakes, *Seism. Res. Lett.,* **76**(1), 40–48.

Clarke, P.J., Paradissis, D., Briole, P., England, P.C., Parsons, B.E., Billiris, H., Veis, G. & Ruegg, J.C., 1997. Geodetic investigation of the 13 May 1995 Kozani-Grevena (Greece) earthquake, *Geophys. Res. Lett.,* **24**(6), 707–710.

Gee, L., Neuhauser, D., Dreger, D., Uhrhammer, R., Pasyanos, M. & Romanowicz, B., 2003. The rapid earthquake data integration project, in *International Handbook of Earthquake and Engineering Seismology,* pp. 1261–1273, eds Lee, W.H.K., Kanamori, H., Jennings, P.C. & Kisslinger, C., Academic Press, San Diego.

Hardebeck, J.L. *et al.*, 2004. Preliminary report on the 22 December 2003, M 6.5 San Simeon, California earthquake, *Seism. Res. Lett.,* **75**(2), 155–172.

Hartzell, S.H. & Heaton, T.H., 1983. Inversion of strong ground motion and teleseismic waveform data for the fault rupture history of the 1979 Imperial-valley, California, earthquake, *Bull. seism. Soc. Am.,* **73**(6), 1553–1583.

Hauksson, E., Jones, L.M. & Hutton, K., 1995. The 1994 Northridge earthquake sequence in California—seismological and tectonic aspects, *J. geophys. Res.,* **100**(B7), 12335–12355.

Hudnut, K.W. *et al.*, 1996. Co-seismic displacements of the 1994 Northridge, California, earthquake, *Bull. seism. Soc. Am.,* **86**(1), S19–S36.

Kaverina, A., Dreger, D. & Price, E., 2002. The combined inversion of seismic and geodetic data for the source process of the 16 October 1999 M_w 7.1 Hector Mine, California, earthquake, *Bull. seism. Soc. Am.,* **92**(4), 1266–1280.

Mai, P.M. & Beroza, G.C., 2002. A spatial random field model to characterize complexity in earthquake slip, *J. geophys. Res.,* **107**(B11), L2308, doi:10.1029/2001JB000588.

Oglesby, D.D. & Day, S.M., 2002. Stochastic fault stress: implications for fault dynamics and ground motion, *Bull. seism. Soc. Am.,* **92**(8), 3006–3021.

Rolandone, F., Dreger, D., Murray, M. & Burgmann, R., 2006. Coseismic slip distribution of the 2003 M_w 6.6 San Simeon earthquake, California, determined from GPS measurements and seismic waveform data, *Geophys. Res. Lett.,* **33**(16), L16315, doi:10.1029/2006GL027079.

Somerville, P.G., Smith, N.F., Graves, R.W. & Abrahamson, N.A., 1997. Modification of empirical strong ground motion attenuation relations to include the amplification and duration effects of rupture directivity, *Seism. Res. Lett.,* **68,** 199–222.

Somerville, P. *et al.*, 1999. Characterizing crustal earthquake slip models for the prediction of strong ground motion, *Seism. Res. Lett.,* **70,** 59–80.

Wald, D.J. & Heaton, T.H., 1994. Spatial and temporal distribution oof slip for the 1992 Landers, California, earthquake, *Bull. seism. Soc. Am.,* **84**(3), 668–691.

Wald, D.J., Heaton, T.H. & Hudnut, K.W., 1996. The slip history of the 1994 Northridge, California, earthquake determined from strong-motion, teleseismic, GPS, and leveling data, *Bull. seism. Soc. Am.,* **86**(1), S49–S70.

Wald, D.J., Quitoriano, V., Heaton, T.H., Kanamori, H., Scrivner, C.W. & Worden, C.B., 1999. TriNet "ShakeMaps": rapid generation of peak ground motion and intensity maps for earthquakes in Southern California, *Earthquake Spectra,* **15**(3), 537–555.

Wills, C.J., Petersen, M., Bryant, W.A., Reichle, M., Saucedo, G.J., Tan, S., Taylor, G. & Treiman, J., 2000. A site-conditions map for California based on geology and shear-wave velocity, *Bull. seism. Soc. Am.,* **90**(6), S187–S208.

Wright, T.J., Parsons, B.E., Jackson, J.A., Haynes, M., Fielding, E.J., England, P.C. & Clarke, P.J., 1999. Source parameters of the 1 October 1995 Dinar (Turkey) earthquake from SAR interferometry and seismic bodywave modelling, *Earth planet. Sci. Lett.,* **172,** 23–37.